

MCPNS: A Macropixel Collocated Position and Its Neighbors Search for Plenoptic 2.0 Video Coding

Vinh Van Duong, Thuc Nguyen Huu, Jonghoon Yim, and Byeungwoo Jeon

Abstract—Recently, it was demonstrated that a newly focused plenoptic 2.0 camera can capture much higher spatial resolution owing to its effective light field sampling, as compared to a traditional unfocused plenoptic 1.0 camera. However, due to the nature difference of the optical structure between the plenoptic 1.0 and 2.0 cameras, the existing fast motion estimation (ME) method for plenoptic 1.0 videos is expected to be sub-optimal for encoding plenoptic 2.0 videos. In this paper, we point out the main motion characteristic differences between plenoptic 1.0 and 2.0 videos and then propose a new fast ME, called macropixel collocated position and its neighbors search (MCPNS) for plenoptic 2.0 videos. In detail, we propose to reduce the number of macropixel collocated position (MCP) search candidates based on the new observation of center-biased motion vector distribution at macropixel resolution. After that, due to large motion deviation behavior around each MCP location in plenoptic 2.0 videos, we propose to select a certain number of key MCP locations with the lowest matching cost to perform the neighbors MCP search to improve the motion search accuracy. Different from existing methods, our method can achieve better performance without requiring prior knowledge of microlens array orientations. Our simulation results confirmed the effectiveness of the proposed algorithm in terms of both bitrate savings and computational costs compared to existing methods. The code of our method can be found at <https://github.com/duongvinh/MCPNS>.

Index Terms—Light field, plenoptic camera, video coding, fast motion estimation, macropixel image.

Vinh Van Duong, Thuc Nguyen Huu, Jonghoon Yim, and Byeungwoo Jeon (corresponding author) are with the Digital Media Laboratory (DMLAB), Department of Electrical and Computer Engineering, Sungkyunkwan University, 2066 Seoburo, Jangan-gu, Suwon, 16410, KOREA (email: bjeon@skku.edu).

This work was supported in part by Basic Science Research Program (RS-2023-00208453) through the National Research Foundation of Korea (NRF) and by the ICT Creative Consilience Program (IITP-2023-2020-0-01821) supervised by the IITP (Institute for Information & communications Technology Planning & Evaluation), both funded by the Ministry of Science and ICT, Korea.

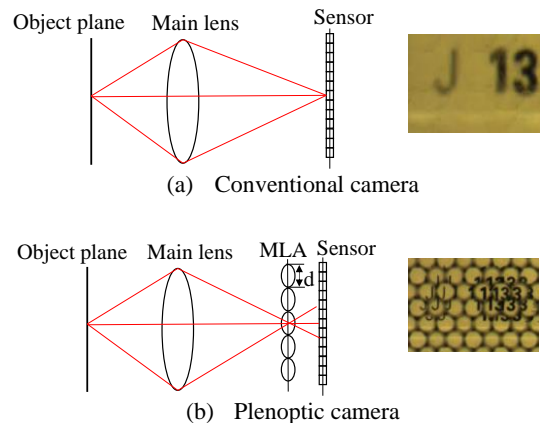


Fig. 1. Illustrations of the conceptual optical structures for conventional and plenoptic cameras. (a) The conventional camera only captures the average intensity of light rays hitting the image sensor, meaning the direction of light rays is lost. (b) With the MLA element, the plenoptic camera can capture both the intensity of light rays and their direction to produce a macropixel image pattern.

I. INTRODUCTION

Light field (LF) imaging contains all directions and intensities of light rays from the scene to an observer, which can be captured by a plenoptic camera. As shown in Fig. 1(a), since a conventional camera only captures the average intensity of light rays hitting the camera sensors, the direction of light rays is lost. In contrast, a plenoptic camera can record not only the intensity but also the direction of light rays due to a microlens array (MLA) placed in front of the image sensor plane, as shown in Fig. 1(b). As a result, the image response in the camera sensor created under MLA is referred to as a macropixel image (MI) or lenslet image. With this unique camera optical structure, the image/video captured by a plenoptic camera provides much richer and more valuable information for applications like depth estimation, refocusing, point cloud data processing, saliency detection, and many more [1].

Since the intensity distribution of plenoptic image/video is quite different from that of conventional image/video, additional care should be paid to effectively reduce spatial and temporal redundancies and maintain good fidelity in plenoptic

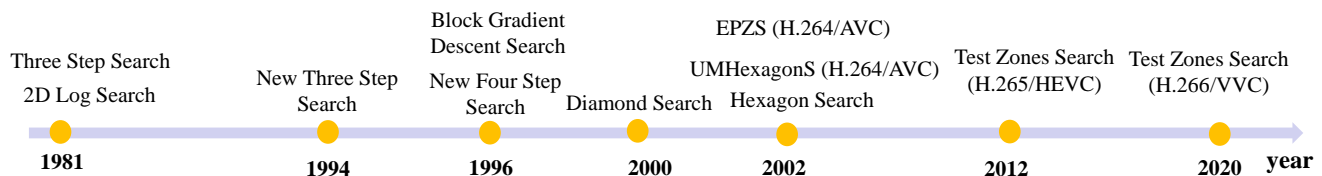


Fig. 2. A diagram of illustrated the milestones of fast motion estimation methods for encoding conventional videos, where the TZS method is currently adopted for the reference software of the most recent standard video encoders, such as H.265/HEVC or H.266/VVC.

image/video [2]-[20]. While a comprehensive survey on coding solutions for plenoptic images can be found in [21]-[22], it is noted that plenoptic video coding has become a new research topic, receiving significant attention from MPEG-Immersive [23]-[25] recently.

More importantly, since the commercial plenoptic 1.0 camera (Lytro Illum) is currently out of the market, the research community is focusing more on plenoptic 2.0 cameras (Raytrix) [26]-[30], which can provide more flexible control of the trade-off between spatial-angular resolutions. Therefore, by considering the distinct intensity distribution of plenoptic 2.0 images, several new intra-coding tools [8]-[9] have been introduced that are designed and targeted for encoding plenoptic 2.0 image. However, inter-coding tools (e.g., motion estimation) for plenoptic 2.0 video have not been well investigated in the literature.

In dealing with video data, especially for compression, motion estimation (ME) is key. This is because ME is an effective tool for finding the best, most similar block in already encoded frames to reduce temporal redundancy. Additionally, the motion vector (MV) is generated by ME; this is denoted as the displacement between the best-matched block and the current prediction. Although Full Search (FS) provides the best quality among various ME algorithms, its computational complexity is very high. Hence, numerous simpler search patterns [31]-[39] have been introduced to overcome the limitations of the FS method, as illustrated in Fig. 2. Recently, the Test Zones Search (TZS) [40] method has been adopted in standard encoders (e.g., H.265/HEVC and H.266/VVC), which has also been the state-of-the-art, fast ME for conventional video. In short, the assumptions related to designing the fast ME method employing TZS for conventional video need to be re-scrutinized for plenoptic video because the complex intensity distribution and motion vectors of plenoptic cameras are different from conventional ones.

Table I presents works related to the fast ME method for plenoptic video coding. In the case of fast ME for plenoptic 1.0 videos, the authors in [46] first proposed macropixel-based fast motion estimation for plenoptic video 1.0 (denoted as MFME), where they suggested that the searching candidates should follow the macropixel collocated position (MCP) search pattern due to its highly optimal motion concentration. Later, they reported the technical proposals [48]-[50] for MPEG-Immersive, which also integrated many coding tools for lenslet video on HEVC. After that, another academic paper described in our previous work [51] proposed microlens-based TZS (MTZS) for plenoptic 1.0 videos, which suggested a searching step in conventional TZS to standardize the microlens image distance. The technical proposal of MTZS in MPEG-Immersive can also be found in [52].

TABLE I

WORKS RELATED TO THE FAST MOTION ESTIMATION METHOD FOR PLENOPTIC VIDEO CODING

Categories	Related Works	
	Technical Proposal for MPEG-Immersive	Academic Papers
Plenoptic 1.0 Videos	[48]-[50], [52]	[46]-[47], [51]
Plenoptic 2.0 Videos	[58]-[60], [62]-[67]	[68]

Regarding fast ME for plenoptic 2.0 videos, a more suitable fast search method should be considered optical structure for plenoptic 2.0 because of its differences from plenoptic 1.0. Taking this into account, several technical proposals [53]-[55] and its academic paper [68] for plenoptic 2.0 videos were introduced recently, which proposed the micro-image-based two-step search (MTSS) method. It includes microlens-diameter and matching-distance spatial search (MMS) as the first step search to exploit the correlation among microlens images due to the distinction of the optical structure of plenoptic 2.0. Additionally, region-limited TZS is employed as the local refinement search in the second step.

In this paper, we observed that the existing approach MTSS described in [68] may still achieve sub-optimal performance in the case of encoding plenoptic 2.0 videos. This is because MTSS employs the matching pixel distance (denoted as s) of plenoptic 2.0 cameras, which exploits the similarity of micro-images spreading over several neighboring microlenses caused by the unfocused MLA structure in plenoptic 2.0 cameras. However, the distance of the matching pixel distance (s) will vary for different video sequences depending on the focused changing of images (e.g., images with different depth of field, disparity, *etc.*). For instance, the real estimated parameter “ s ” is for each video sequence is reported in [68]. Hence, this method might not handle video sequences with complex scenes or complex motion (e.g., video sequences with different depths of field or fast motion generated by camera/object moving). Although there are several updates and improvements with more accurate parameters of the MTSS method which are reported in their technical proposal for MPEG-Immersive [63], the pre-defined search candidates in MTSS still limit the efficiency of this method.

Motivated by the above observations, we note that the problem of fast ME for plenoptic 2.0 videos is more difficult compared to traditional plenoptic 1.0 videos. Because the plenoptic 2.0 cameras with more complex optical structure generated more complex motion behavior. To this end, we propose a new macropixel collocated position and its neighbors

search for plenoptic 2.0 video coding (denoted as MCPNS). Specifically, by conducting statistical analysis of the motion distribution of plenoptic 2.0 videos, we also observe the optimal MV distribution to be mainly around MCP locations. However, we point out that there is a large portion of optimal MV deviation around each MCP in the case of plenoptic 2.0 videos. Taking this into account, we propose a joint search approach by adding extra neighbors search candidates around each MCP location in order to handle the large MV deviation problem resulting from the optical structure of plenoptic 2.0 cameras. This is the main distinction from existing methods (MFME [46] or MTSS [68]), which allows us to capture more accurate optimal MV at the macropixel level searching stage in the case of plenoptic 2.0 videos. It is a simple yet effective method compared to other methods, based on our rigorous analysis and understanding of the motion characteristics of plenoptic 2.0 videos. Moreover, the idea of a joint search approach at the macropixel level searching stage is conceptually novel since there are no existing academic papers on fast ME for plenoptic 2.0 videos that clearly provide theoretical and statistical analyses of the motion difference between plenoptic 1.0 and 2.0 videos.

Preliminary results of this paper are reported in [62][67], where the neighbors MCP search concept was introduced in [62] helping to improve motion accuracy, and the fast MCP search pattern based on center-biased assumption at macropixel level was introduced in [67] helping to reduce encoding time. In this paper, by considering the trade-off between the coding performance and encoding time complexity, we provide comprehensive results and analysis of our proposed method. In short, the contributions of our paper are summarized as follows:

- Different from existing methods, we theoretically discuss the main assumptions on the effects of scene motion captured by plenoptic cameras. To validate these assumptions, we also provide a statistical analysis of the MV distributions for both conventional and plenoptic videos and point out the main differences between them.
- We present a new fast ME called MCPNS, which contains a joint search approach between MCP and its neighbors MCP search locations to handle the large motion deviation at the macropixel level search stage in the case of plenoptic 2.0 videos.
- To reduce the time complexity of ME in the case of a large window search, we introduce a fast MCP search pattern based on motion center-biased assumption and fast neighbors MCP search only for the top K -MCP position containing the lowest distortion cost.
- Moreover, our method is more generalized by performing the MLA orientation-agnostic MCP search pattern to address different MLA orientations of plenoptic 2.0 cameras.

The remainder of this paper is organized as follows. First, Section II presents the 4D LF motion properties and the motion distribution characteristics of each plenoptic camera model. Then, Section III presents our proposed fast search MCPNS for plenoptic 2.0 video coding in detail. Finally, Section IV evaluates the performance, and our conclusions are given in Section V.

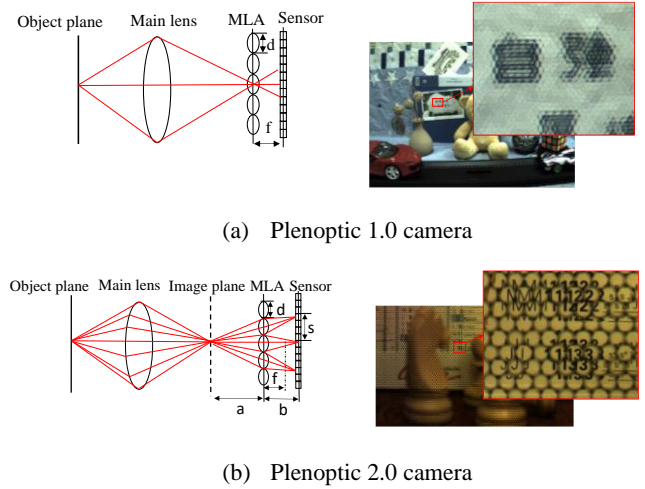


Fig. 3. The optical structures and real macropixel images captured by plenoptic 1.0 and plenoptic 2.0 cameras [8], [42].

II. 4D LIGHT FIELD MOTION PROPERTIES AND ITS STATISTICAL ANALYSIS

This section presents background information related to different optical structures of plenoptic camera model and light field motion characteristics of the light field recorded in a 4D LF sensor camera. After that, we analyze the statistical MV distribution between conventional and plenoptic videos and point out the main differences between them.

A. Structure and Characteristics of Plenoptic Cameras

As shown in Fig. 3(a), the plenoptic 1.0 camera has the MLA placed at the image plane of the main camera lens, with the photosensor camera located at one focal length behind the microlens. Therefore, the main camera lens is focused on a distance of one focal length in front of the microlens and the MLA is focused at infinity. As a result, all pixels under the microlens correspond to a single spatial object point, which comes from a specific direction to that pixel, as shown on the right side of Fig. 3(a). Hence, images from the plenoptic 1.0 camera are rendered by integrating all angular samples at a particular spatial point. However, since each spatial point is sampled by a single microlens, rendering involves integrating all of the pixels in each micro-image. As designed, we only can take one pixel per microlens in the case of plenoptic 1.0, resulting in a rendered image with very low resolution.

Different from the plenoptic 1.0 camera, the plenoptic 2.0 camera is based on a microlens array focused on the image plane of the main lens, as shown in Fig. 3(b). Thus, each microlens captures a portion of the image formed by the main lens. We can think of the sensor as being moved back, away from the main lens, so the image is formed some distance in front of the microlenses. As a result, the MLA serves as an array of real cameras, reimaging parts of the image onto the sensor. In this respect, each microlens forms a relay imaging system with the main camera lens. The position of each microlens satisfies the lens equation, $1/a + 1/b = 1/f_m$, where a is the distance between the MLA and the image plane of the main lens, b is the distance between the MLA and camera sensor, and

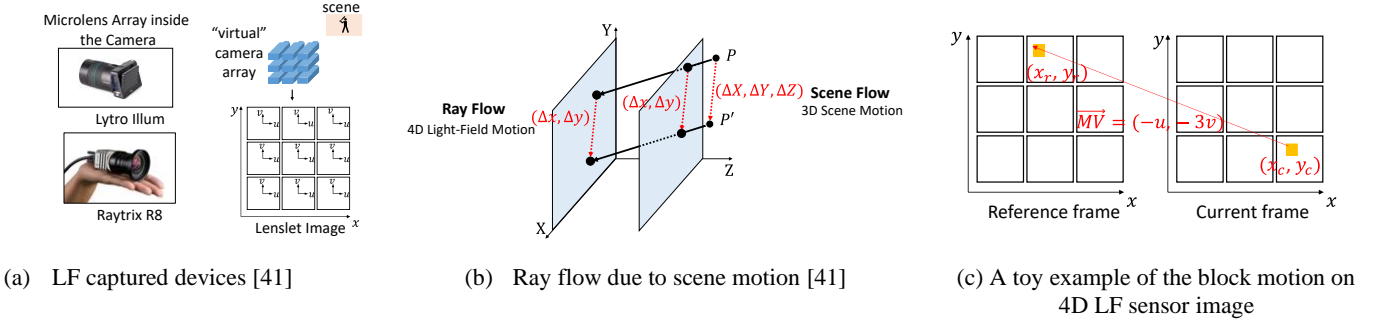


Fig. 4. Illustration of ray flow due to scene motion in a light field camera sensor image. (a) Plenoptic cameras with the microlens array work like a virtual camera array system. (b) Motion of the scene point that emits or reflects the ray results in a change in the (x, y) coordinates of the ray, but the (u, v) coordinates remain constant. (c) A toy example to show the block motion (translation) in the current frame at (x_c, y_c) to the reference frame at (x_r, y_r) with step sizes of u and v in vertical and horizontal coordinates.

f_m is the focal length of the microlens. According to the geometric distance, the distance between the pixel's response on the sensor from the same object point, denoted as s , is calculated using equation (1) for plenoptic 2.0 using Keplerian mode (Raytrix R5 and Raytrix R8 cameras) or using equation (2) for plenoptic 2.0 using Galilean mode (Tsinghua Single Focused camera) as follows [8]:

$$s = \frac{a - b}{a} \times d \quad (1)$$

$$s = \frac{a + b}{a} \times d \quad (2)$$

Here, d is the diameter of each microlens, depending on the plenoptic camera model. With the new optical design of the plenoptic 2.0 camera compared to plenoptic 1.0, several key conclusions can be made:

- The key difference here is that, due to the relay image system in plenoptic camera 2.0, the spatial-angular resolution is not fixed by the number of microlenses. This means that the angular samples for a given spatial point are sampled by different microlenses, which enables higher spatial resolution compared to plenoptic 1.0. In other words, rendering with the plenoptic 2.0 camera data involves integration across microlens images rather than within microlens images, as is done in plenoptic 1.0. As a result, the plenoptic 2.0 camera can capture LF images with much higher spatial resolution compared to the plenoptic 1.0 camera.
- Additionally, since there is a major difference between the optical structure of plenoptic 1.0 and 2.0 cameras, we need to pay attention to their pixel intensity distributions, which helps us to design a more effective search algorithm that is suitable for each type of camera. In short, plenoptic 2.0 video coding is a new topic that has received significant attention from MPEG-I [26]-[30], [56]-[57]. However, it still needs further investigation in order to design an effective coding method to efficiently compress these kinds of data according to different acquisition devices.

B. Effect of Scene Motion on Ray Motion Recorded on Plenoptic Camera Sensors

In this section, we briefly revisited the ray flow equation proposed in [41], which describes the relationship between the *scene flow* (3D scene motion) and the *ray flow* (ray motion recorded in a sensor camera). In short, we can interpret how the

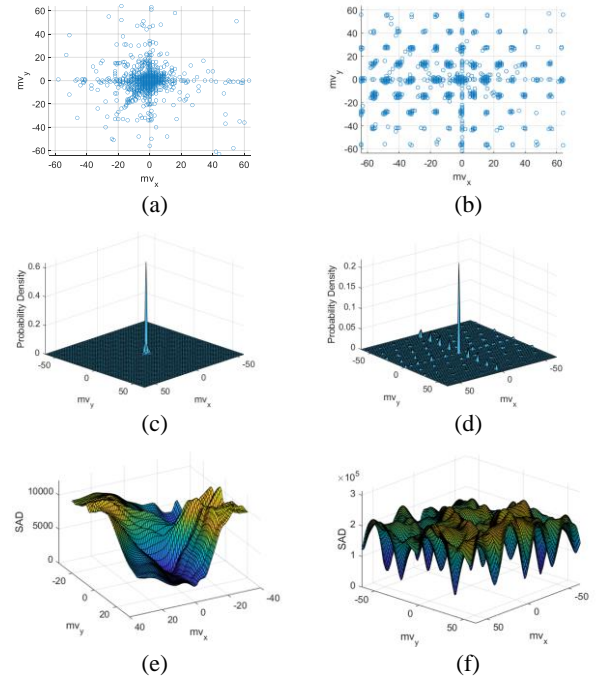


Fig. 5. Illustration of typical MVs distribution and matching error surface between conventional (left side) and plenoptic (right side) videos: the MV distribution map (first row), the probability density distribution of MV (second row), and the matching error surface distribution (third row).

ray flow as the change $(\Delta x, \Delta y)$ in a light ray coordinate due to the scene motion change $\Delta \mathbf{X} = (\Delta X, \Delta Y, \Delta Z)$ 3D space coordinates. Moreover, since our goal is to estimate the 2D motion vector in block-based video coding, which is simpler than estimating the dense 3D scene flow in the original work [41], we mainly rely on these important properties of the ray flow equation to gain intuitions and insights into our video coding problem.

In detail, given the 3D scene point P at the location \mathbf{X} and the time instance t , we denote that $\mathbf{X}' = \mathbf{X} + \Delta \mathbf{X}$ is the location of point P at the time instance $t + 1$, where $\Delta \mathbf{X} = (\Delta X, \Delta Y, \Delta Z)$ is the difference between 3D scene point locations. The main assumption is that if we only consider the translation motion of the scene patch, the rays are moving parallel to themselves (*i. e.*, (u, v) coordinates of the ray remain constant).

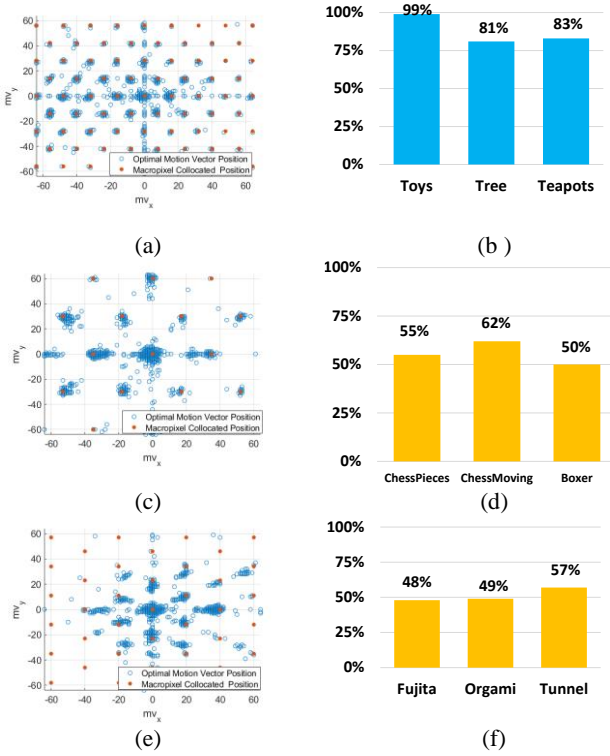


Fig. 6. Statistical analyses of MV distributions of a plenoptic 1.0 camera (Lytro Illum; in the first row) and plenoptic 2.0 cameras (Raytrix R8 and Raytrix R5; in the second and third rows, respectively). The MVs are plotted together with MCP locations (denoted as red points) in the first column, and the proportion of the optimal MV located at the same location as MCP is shown in the second column.

As shown in Fig. 4(a), we represent a 4D LF sensor image as a 2D array of pinhole cameras (i.e., a 2D array of microlens). In this representation, we denote (u, v) as the pixel indices within individual microlens and (x, y) represent the location of the cameras. To be self-contained, we recap the main assumptions of 3D scene motion recorded in sensor images of plenoptic cameras, which can be found in [41], as follows:

- As shown in Fig. 4(b), a light ray shifts horizontally or vertically across microlens images, where the amount of shift $(\Delta x, \Delta y)$ is independent of the ray's original coordinates. In other words, rays maintain the same pixel index (u, v) after motion but in different microlens images (x, y) ; this is the case because the scene motion results in rays being translated parallel to themselves. This is the *most important characteristic* that we need to pay attention to, which is highlighted by the key difference between scene motions recorded with the 2D conventional sensor image versus our 4D LF sensor image.
- As shown in Fig. 4(c), we illustrate a toy example of translation motion on the 4D LF sensor camera, where we can see that block motion only changes in the (x, y) coordinates; the (u, v) coordinates remain unchanged (i.e., moving with a **step size of u and v** in horizontal and vertical coordinates). Based on this fundamental observation, we will analyze the motion vector distribution for a real video captured by a plenoptic camera and discuss insightful observations to design an

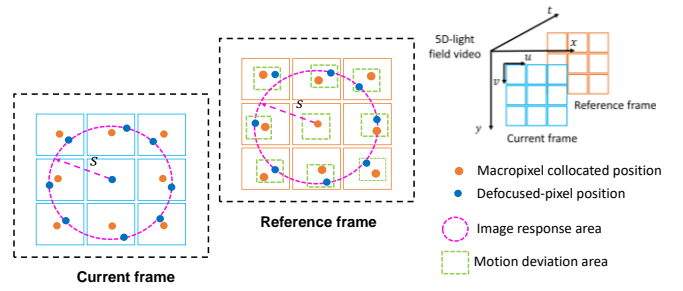


Fig. 7. A toy example illustrates different types of pixel similarity that can be found by the motion estimation process, where we can see that the inter-pixel similarity varies in a larger angular window search range for the case of plenoptic 2.0 videos.

effective search pattern for each type of plenoptic camera model.

C. Statistical Analysis and Motivation

To analyze the differences in motion characteristics between conventional and plenoptic videos, the VVC reference software VTM-11.0 [58] is used for encoding. In the case of conventional video, several standard video sequences are tested, and their detailed properties are described in the common test condition document [45]. For plenoptic video test sequences, we use the video sequences that were captured by three different kinds of plenoptic cameras, (Lytro Illum, Raytrix R5, and Raytrix R8, respectively). We encode the first 30 frames of each test sequence using the default configuration in the low-delay main (LD-main) profile. The Full Search is used to obtain the optimal MV with a search range (SR) of 64. Our main observations are presented in detail below.

Unique motion distribution of plenoptic videos compared to conventional videos: From Figs. 5(a)-(d), we can see that the MV distribution of conventional video is mostly located at the center search area, where the distribution of motion in the case of a plenoptic camera is sparsely located around the search window. Due to the MLA elements, the global motion generated by object movement is captured by MLA at a resolution equal to the nearest distance between these microlenses. Moreover, in Figs. 5(e)-(f), we plot the sum absolute difference (SAD) in the block matching process, which gives us the difference in the intensity distribution between conventional and plenoptic test sequences. It can be seen that the uni-modal error surface is no longer valid in the case of the plenoptic video. In short, since the TZS method designed based on these assumptions is no longer effective in encoding the plenoptic videos, the TZS performs much worse in the case of coding plenoptic videos. Hence, this motivated us to design a new fast search pattern for plenoptic videos.

Optimal motion vectors are located mainly at macropixel collocated positions (MCPs): In the first column of Fig. 6, we plot the optimal MVs together with the MCP locations for different camera models, where each red dot corresponds to the location of one microlens in MLA placed in front of the camera sensor. Moreover, it should be noted that the MLA layout arrangement is different according to each plenoptic camera version. For instance, the Lytro Illum and Raytrix R8 cameras have a horizontal MLA layout arrangement, whereas the

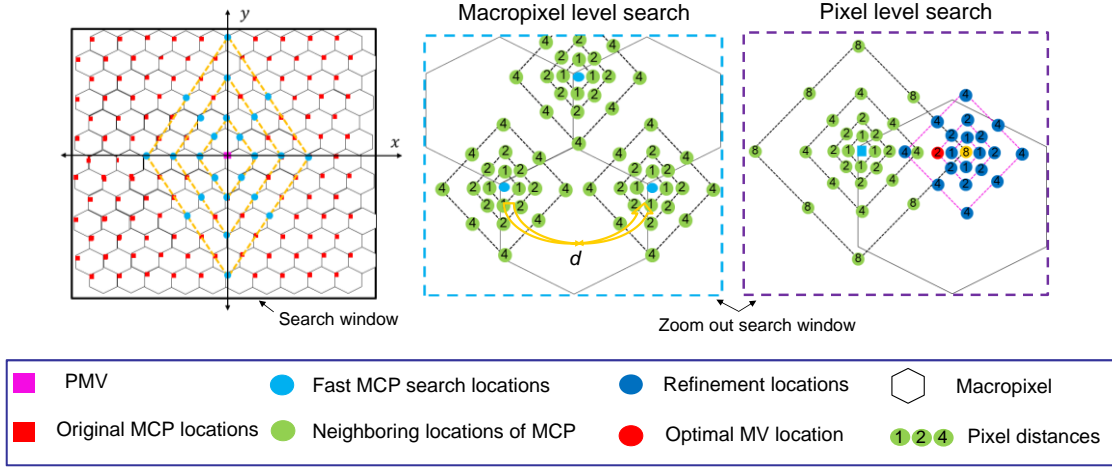


Fig. 8. Illustrations of search patterns in our proposed method to address the motion characteristic of plenoptic 2.0 videos at macro-pixel search level and pixel search level, respectively.

Raytrix R5 has a vertical MLA layout arrangement. From these results, we notice that the optimal MVs are mainly located around the MCP points and sparsely distributed all over the search window; this is different from conventional MV, which are only located around the predicted motion vector pMV (i.e., located around the center of the window search area). Additionally, we try to calculate the percentage of optimal MVs located exactly at MCP locations in the second column of Fig. 6. Specifically, optimal MVs are highly located exactly at MCP locations (about more than 80%) for plenoptic 1.0 (Lytro Illum), whereas this is much lower for the plenoptic 2.0 cameras: about 50% to 60% for Raytrix R8 and R5 camera models, respectively. Several observations can be made as follows. For example, because optimal MVs are mainly concentrated at these MCPs, we can select these MCPs as the search candidates in the initial search instead of using the diamond search (as done in the TZS method).

A large portion of motion deviation around each MCP search location in case of plenoptic 2.0 videos: More importantly, since the optical structure is different between plenoptic 1.0 and plenoptic 2.0 cameras, a significant deviation is observed between the optimal MVs and these MCPs in plenoptic 2.0; the deviation is smaller for plenoptic 1.0. Moreover, this is a good clue that demonstrates why the MFME[46]/MTSS[68] will not be effective when we apply this fast search for encoding our plenoptic 2.0 videos. In other words, if we only perform the search process on these MCPs, as is done in MFME[46]/MTSS[68], this cannot guarantee that we will find an optimal MV. The percentage of optimal MVs located at exactly these MCP locations in the case of plenoptic 2.0 is much less compared to the case of plenoptic 1.0.

In short, the large motion deviation around each MCP location is the most important and unique motion characteristic of plenoptic 2.0 videos compared to plenoptic 1.0 videos. This difference should be paid attention to in order to utilize the best design of our method. In Fig. 7, we further illustrate another toy example to help us better understand the similarity of pixels in the motion search process in plenoptic 2.0 video coding. Since each microlens is treated as a “virtual camera” that records the same scene from a different perspective, the pixel similarity of micro-image might be easily found in a neighboring microlens

by following the macropixel distance values, as denoted as orange color in Fig. 7. However, because the plenoptic 2.0 camera is unfocused camera, meaning that each microlens records part of an object and creates the defocused microlens imaging pattern in camera sensor. The defocused micro-image is spreading over several neighboring microlenses following the matching distance (s) as shown in Eqs (1) and (2). More importantly, the matching distance (s) is not fixed, where it will vary depending on the characteristics of each video sequence (e.g., disparity range, depth of field, etc.).

Finally, the inter-pixel similarity in the case of plenoptic videos is mainly affected by object movements, where the movement occurs with a step size of u and v in horizontal and vertical coordinates. However, the inter-pixel similarity in the case of plenoptic 2.0 is further affected by larger defocused-pixel similarity variation. That is, we can see that the inter-pixel similarity block in the case of plenoptic 2.0 varies over a larger search window, as illustrated in Fig. 7. This will cause a large and complex motion deviation when we carry out the motion search in the reference image looking for the best-matched block in the case of plenoptic 2.0 videos. In the end, this information has motivated us to design a new search pattern to handle the larger motion deviation around each MCP location in the case of motion estimation of plenoptic 2.0 videos.

III. PROPOSED METHOD

In this section, we introduce the proposed search patterns in each searching stage in detail, which describes how our method can estimate more accurate block motion vectors compared to state-of-the-art methods.

A. Search Locations Addressing Highly Optimal Motion Vectors Located at Macropixel Collocated Positions (MCPs)

Original MCP Search Pattern. As pointed out in Section II.B, the motion distribution of plenoptic videos is mainly located at MCP locations, where the light rays shifted across microlenses generating the motion displacement at the macropixel resolution. To reflect this unique characteristic, we found that the motion search pattern at the very first step should follow these MCP locations. This is because the main difference in motion characteristic of plenoptic videos compared to

conventional videos is that the block motion is shifted in one or multiple macropixel resolution distances in the case of plenoptic videos, whereas the block motion in conventional videos is only shifted in the pixel resolution distance (e.g., as can see in Fig. 4). This means a search pattern designed in TZS method for the conventional motion search in the pixel level resolution distance will be insufficient to cover the bigger motion moving step at macropixel level resolution in plenoptic videos.

As shown in Fig. 8, we can derive the MCP locations from the center of search window by following the macropixel diameter (d). For simplicity, we will describe how to define the position of MCP candidates in the horizontal MLA orientation, where the process will be similar for the case of vertical MLA orientation. In detail, let us denote $h = \sqrt{3}d/2$ and $w = d$ as the distance between two adjacent microlenses in the horizontal and vertical directions. Given the window search range (W), the MCP search candidates can be derived by using equations (3), as follows [46],[68]:

$$\begin{cases} x = p \cdot w + \frac{w}{2}, & q \in O \\ y = q \cdot h, & q \in E \end{cases} \quad (3)$$

with $p \in \Phi, q \in \Psi$, and $(x, y) \in [-W, W]$

Here, (x, y) represent the coordinates of each MCP candidate within the search range. Additionally, O and E represent sets of odd and even numbers, respectively. Additionally, (Φ, Ψ) denote the set number of microlenses inside the searching range area (W) in the horizontal and vertical coordinates. Moreover, the total number of MCP candidates inside the given search range is calculated as follows [46],[68]:

$$\psi_1 = \begin{cases} (m+1) \cdot \left(2 \left\lfloor \frac{W}{w} \right\rfloor + 1\right) + 2m \left\lfloor \frac{W+w/2}{w} \right\rfloor, & m \in E \\ m \cdot \left(2 \left\lfloor \frac{W}{w} \right\rfloor + 1\right) + 2(m+1) \left\lfloor \frac{W+w/2}{w} \right\rfloor, & m \in O \end{cases} \quad (4)$$

$$m = \left\lfloor \frac{W}{h} \right\rfloor$$

Fast MCP Search Pattern Addressing the Center-biased Assumption at Macropixel Level. As illustrated in Fig. 9, instead of checking all MCPs locations as defined in equation (3), we propose a fast MCP search pattern that allows us to speed up encoding time, especially in case of a large search window. Specifically, we observed that the optimal MV density distribution in the plenoptic video is followed by the center-biased assumption at the macropixel level resolution, which is the key difference compared to the MV distribution in the conventional video followed by the center-biased assumption at pixel level resolution. Specifically, the number of MCP search candidates in our method is calculated as follows:

$$\hat{\psi}_1 = \sum_{i=1}^M 8, i \leq M \text{ with } M = \left\lfloor \frac{W}{d} \right\rfloor, \quad (5)$$

where W and d respectively denote the search window and microlens diameter. Besides, since the macropixel distance is already very large, it is important to note that the searching step is increased to the maximum value of M following the linear

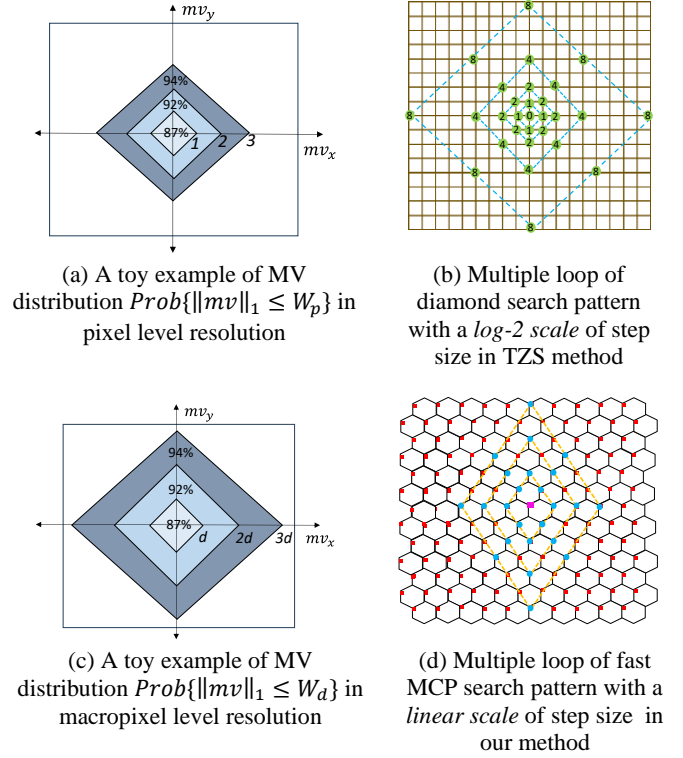


Fig. 9. Illustration of the MV density distribution following the center-biased assumption at pixel level resolution and macro-pixel level resolution at the top and bottom, respectively.

scale order compared to \log_2 scale order as done in TZS method.

MLA Orientation-Agnostic MCP Search Pattern Addressing Different MLA Orientation. Fig. 10 shows two kinds of MCP patterns depending on the MLA orientation. The MLA arrangement is not necessarily the same over LF cameras. For example, the MCP locations of the Raytrix R8 camera follow the horizontal MLA orientation of Fig. 10(a), while that of the Raytrix R5 and Single-Focused camera models follow the vertical MLA orientation in Fig. 10(b). Taking this into account, our method in previous contribution [62], [67] requires knowledge of MLA orientations in advance in order to properly predefine the MCP search locations, whereas the MTSS [68] needs to rotate the given image by 90° in clockwise through pre-processing if the MLA orientation is not horizontally arranged as in Raytrix R5 and Single Focused camera. In short, our MCPS2.0 [62], [67] and MTSS [68] need prior knowledge of MLA orientation or preprocessing of rotation before performing actual motion estimation procedure.

To make things more complex, camera users actually have full freedom to take photos in portrait-mode or landscape-mode. Thus it may be practically not feasible to assume that the MLA orientation of a given LF image is known in advance. Moreover, when the video is edited by mixing several sources or cuts to form a picture, the MLA orientations inside one picture cannot be even assumed to be the same. In this respect, it is noted that the conventional fast ME method (e.g., Test Zones Search (TZS) [58]) is also agnostic to camera or content orientation, that is, it does not require prior information on whether the video was captured either in portrait or landscape

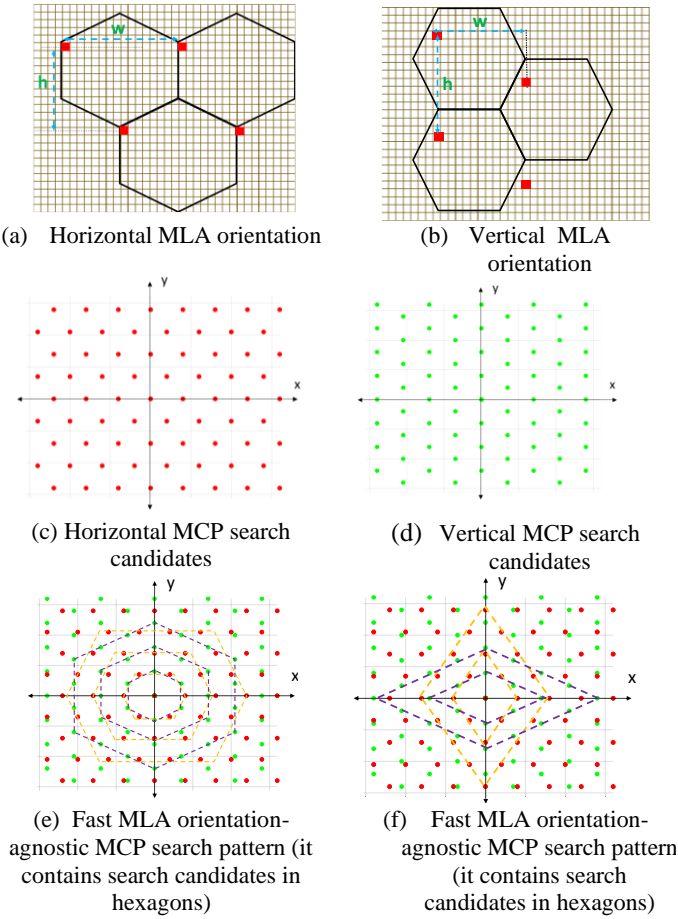


Fig. 10. Illustrations of our proposed fast MLA orientation-agnostic MCP search pattern which can accommodate either MLA layout of horizontal or vertical MLA orientations in various plenoptic 2.0 camera model.

mode. Hence, it is better to design a fast motion search algorithm for LF video which is agnostic to MLA orientation. For example, ψ_1 has 1307 original MCP locations which are derived from its center of predicted MV for Raytrix camera R5 with $d = 23$ and $W = 384$. By using our fast MLA orientation-agnostic MCP search locations, the actual fast MCP candidates is significantly reduced (e.g., $|\hat{\psi}| = \lfloor \frac{384}{23} \rfloor \times 8 = 128$). Since we need to perform the search in both horizontal and vertical rhombus orientations, the number of fast MCP candidates is increased by double (e.g., $\hat{\psi} = 2 \times \lfloor \frac{384}{23} \rfloor \times 8 = 256$). It should be noted that the number of fast MCP candidates is much smaller than its original MCP locations (i.e., $|\hat{\psi}| \ll |\psi_1|$).

B. Search Locations Addressing Large Portions of Optimal Motion Vector Deviation Around Each MCP

Neighbors MCP Search Pattern. Motivated by our observation in Section II.B, we propose a neighbors MCP search in our method, which enables to handle a large motion deviation around these MCP locations in case of plenoptic 2.0 videos. Specifically, the number of neighboring candidates at each MCP location is calculated as follows:

$$\psi_2 = 4 + \sum_{i=2}^N 8, i \leq N \text{ with } N = \log_2(d), \quad (6)$$

where i depends on the searching distance in N loops of the diamond search. The search window of the neighbors MCP search is equal to size of the microlens diameter (d). This algorithm uses the small diamond shape consisting of four checking points for the first loop and the large diamond shape with eight checking points for the remaining loops. As shown in Table II, there is high percentage of optimal MV varying around each MCP location within a search window of 8-pixel distance. Therefore, if we cannot find a new best MV within 8-pixel distance (i.e., every three-searching step), we will apply the early terminated strategy to remove the redundant search. That is, the search will stop if the search process cannot find a new minimum BMD point after every checking three searching loops.

Fast Neighbors MCP Search Approach. A straightforward approach is to perform the neighbors MCP search at all MCP locations, which leads to an unexpected computational power to perform this step. Therefore, instead of performing the neighbor search at all fast MCP locations ($\hat{\psi}_1$), we select the top K number of MCP candidates among $\hat{\psi}_1$ MCP locations with the lowest BMD values to perform the neighbors MCP search. For example, in this paper, we empirically set $K = 16$, which is much smaller compared to the original fast MCP locations (e.g., $\hat{\psi}_1 = 256$ in the last step). The neighbors MCP search will be performed at each MCP position sequentially until reaching the last K MCP locations. The total search points at this neighbors MCP search step is equal to $K \times \psi_2$.

After obtaining the best MV at the macropixel motion resolution level, we need to further search the motion over a smaller grid around the current best MV candidate, as shown in Fig. 8. In this paper, the star-based refinement search pattern proposed in TZS [58] for conventional video coding is adopted for our pixel motion resolution search. The number of search candidates needed in the best case is calculated as:

$$\psi_3 = 4 + \sum_{i=2}^N 8, i \leq N \text{ with } N = \log_2(d), \quad (7)$$

Here, i depends on the searching distance in N loops of the diamond search. Moreover, it is important to note that we only added extra $\hat{\psi}_1$ MCP candidates from another MLA orientation compared to eq. (4), as follows:

$$\Omega = 2\hat{\psi}_1 + K\psi_2 + \psi_3 \quad (8)$$

To make our method conceptually easier to understand, Fig. 11 present the whole procedure of our proposed algorithm, where the key idea/concept of selected search candidates in different fast search methods can be found in supplemental file.

IV. EXPERIMENTAL RESULTS AND ANALYSIS

In this section, we first describe the test conditions in detail. Then, the coding performance in terms of compression efficiency, computation complexity, and ablation study are provided in detail.

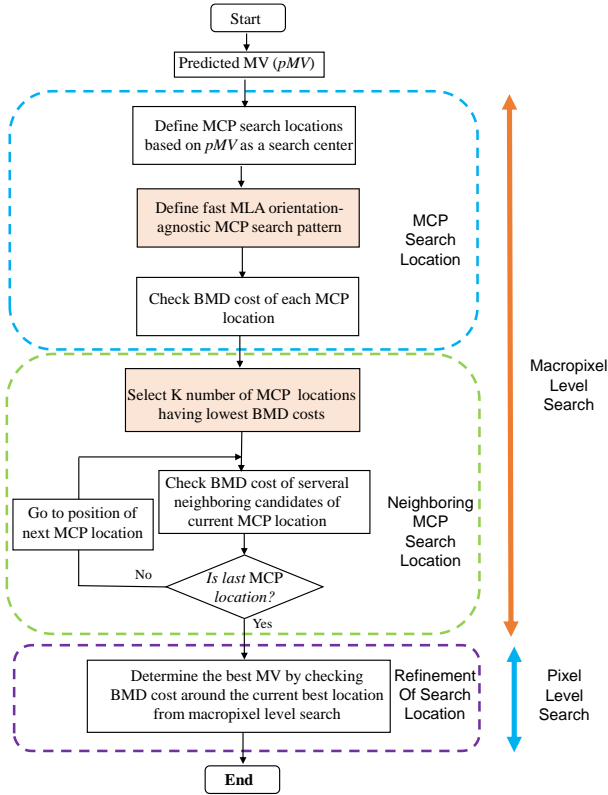


Fig. 11. An illustration of the whole procedure of our proposed method, where the fast search decision in each searching location is highlighted in orange color.

A. Test Conditions

As shown in Fig. 12, we use eleven plenoptic 2.0 videos from the MPEG-I public dataset [59]-[60], which were captured by two kinds of plenoptic 2.0 cameras: Raytrix R5, Raytrix R8, and Single Focused camera models. All the test videos contain the first 30 frames of these videos. The proposed algorithm and other anchor methods are implemented on top of VVC reference software VTM 11.0 [58] with quantization parameters in common test conditions (CTC) [59]. We performed these experiments on servers with the Windows 10 operating system, ADM Ryzen 9 3900X 12-Core Processor, and 32GB DDR4 memory. We encoded and evaluated the performance under default settings in low-delay main (LD-Main) and random access-main (RA-Main) configurations. The rate-distortion (RD) performance is evaluated in terms of the Bjøntegaard delta bitrate (BDBR) [61], where a negative BDBR value denotes better compression performance compared to the anchor method. The peak signal-to-noise ratio (PSNR) in the BDBR is measured in the Y channel color (Y-BDPSNR). In addition, the encoding time ratio computed for each video sequence as follows:

$$Enc\ Time\ Ratio = \frac{geomean(T_m)}{geomean(T_{anchor})} \times 100 \quad (9)$$

Here, T_m and T_{anchor} denote the geometric mean of the encoding time in four quantizations of method m and the anchor method.

To evaluate the effectiveness of our proposed method, we define several testing cases in Table III. In addition to the TZS

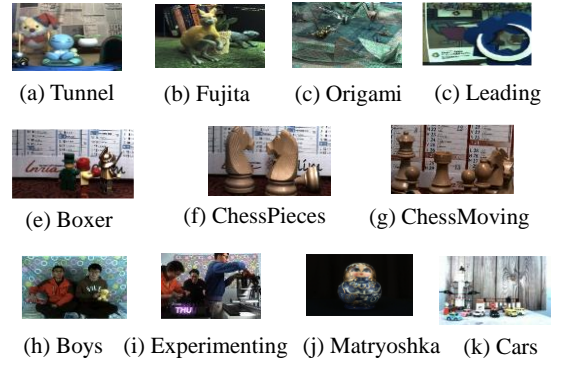


Fig. 12. The plenoptic 2.0 video sequences. (a)-(d): Raytrix R5 captured video sequences, (e)-(g): Raytrix R8 captured video sequences, and (h)-(k) Single Focused captured video sequences.

TABLE III
THE CODING SETTING OF TESTING CASES; OUR PROPOSED METHOD IS HIGHLIGHTED IN **BOLD**.

TESTING CASES	CODING TOOL CONFIGURATION SETTINGS
VVC	VTM 11.0 [58] with Main Profiles
FS	“VVC” + Full Search method [58]
TZS	“VVC” + TZS method [58]
MFME	“VVC” + MFME [46]
MTSS	“VVC” + MTSS [68]
MCPNS	“VVC” + Our proposed MCPNS

and FS methods, we compare our method with several state-of-the-art fast MEs for plenoptic videos, including the MFME [46] for plenoptic 1.0 videos and MTSS [68] for plenoptic 2.0 videos. It should be noted that the MFME [46] was originally designed for encoding plenoptic 1.0 video sequences in HEVC reference software, but we have re-implemented this method in the VVC platform and modified it by setting the diameter of the microlens parameter according to the type of plenoptic 2.0 video sequence. Additionally, the results of MTSS were also generated using the executable file provided by its authors. For making a fair comparison, all methods (FS, MFME [46], MTSS [68], and our MCPNS) only replaced the TZS method in the uni-predictive search process. That is, the performance of FS is optimal. This helps us better understand the maximum performance that each method can achieve when compared to FS method.

B. Overall Performance of Proposed Methods

Tables IV and V show performance comparisons of our proposed method and other methods in LD-Main and RA-Main conditions. Moreover, we present the comparison results with existing fast ME for plenoptic videos in two scenarios: with or without prior information on MLA orientation. From these results, we can observe several key conclusions as follows:

- Our method outperforms the TZS method by an average of 3.37%/2.54% in the LD-Main and RA-Main profiles, respectively. This is because due to the ineffective search location and searching strategy, which was originally designed for conventional video, the TZS algorithm suffers a significant loss in coding performance compared to our

TABLE IV

THE PERFORMANCE COMPARISON OF FAST ME METHODS USING IN UNI-PREDICTIVE ME SEARCH WITH LD-MAIN CONDITIONS.

Camera model	Sequences	Agnostic to MLA Orientation	Without Prior Information of MLA Orientation			With Prior Information of MLA Orientation**		
		FS	MFME	MTSS*	MCPNS	MFME	MTSS*	MCPNS
Raytrix R5	Tunnel	-3.82%	1.37%	-2.81%	-3.38%	-3.62%	-	-3.62%
	Fujita	-8.88%	4.85%	-3.85%	-3.62%	-7.15%	-	-8.34%
	Origami	-6.13%	2.71%	-0.96%	-8.34%	-5.05%	-	-5.23%
	Leading	-2.88%	5.49%	-1.59%	-5.23%	-2.65%	-	-2.68%
Raytrix R8	Boxer	-3.35%	-2.90%	-2.58%	-2.68%	-2.90%	-2.58%	-3.19%
	ChessPieces	-8.01%	-7.53%	-7.60%	-3.19%	-7.53%	-7.60%	-7.50%
	ChessMoving	-5.08%	-3.41%	-3.67%	-7.50%	-3.41%	-3.67%	-4.03%
Single Focused	Boys	-0.85%	4.94%	0.21%	-4.03%	-0.53%	-	-0.65%
	Experiments	-1.01%	2.60%	-0.04%	-0.72%	-0.59%	-	-0.77%
	Cars	-0.24%	0.01%	0.00%	-0.77%	0.01%	-	-0.21%
	Matryoshka	-1.20%	1.88%	-0.38%	-0.18%	-0.86%	-	-0.80%
Avg. BD-rate		-3.77%	0.91%	-2.12%	-3.37%	-3.12%	-	-3.37%
Avg. Enc. Time		410%	99%	101%	105%	99%	-	105%

*The results generated using an executable file provided by the authors, it only gives the best performance in case of sequences with the horizontal MLA orientation

** It assumes that the videos sequences captured by plenoptic camera with the horizontal MLA orientation

TABLE V

THE PERFORMANCE COMPARISON OF FAST ME METHODS USING IN UNI-PREDICTIVE ME SEARCH WITH RA-MAIN CONDITIONS.

Camera model	Sequences	Agnostic to MLA Orientation	Without Prior Information of MLA Orientation**			With Prior Information of MLA Orientation		
		FS	MFME	MTSS*	MCPNS	MFME	MTSS*	MCPNS
Raytrix R5	Tunnel	-3.52%	0.37%	-2.93%	-3.38%	-3.43%	-	-3.38%
	Fujita	-4.02%	1.92%	-1.27%	-3.97%	-3.00%	-	-3.97%
	Origami	-5.40%	1.45%	-2.70%	-4.51%	-4.41%	-	-4.51%
	Leading	-3.71%	1.68%	-2.53%	-3.75%	-3.34%	-	-3.75%
Raytrix R8	Boxer	-2.11%	-1.63%	-1.68%	-1.90%	-1.63%	-1.68%	-1.90%
	ChessPieces	-4.71%	-4.41%	-4.33%	-4.64%	-4.41%	-4.33%	-4.64%
	ChessMoving	-4.86%	-3.38%	-4.19%	-4.75%	-3.38%	-4.19%	-4.75%
Single Focused	Boys	-0.45%	2.57%	0.21%	-0.25%	-0.22%	-	-0.25%
	Experiments	-0.87%	1.40%	-0.04%	-0.64%	-0.50%	-	-0.64%
	Cars	-0.02%	-0.03%	0.01%	-0.03%	0.01%	-	-0.03%
	Matryoshka	-0.81%	1.04%	-0.11%	-0.08%	0.27%	-	-0.08%
Avg. BD-rate		-2.77%	0.09%	-1.78%	-2.54%	-2.19%	-	-2.54%
Avg. Enc. Time		1040%	100%	107%	103%	99%	-	103%

*The results generated using an executable file provided by the authors, it only gives the best performance in case of sequences with the horizontal MLA orientation

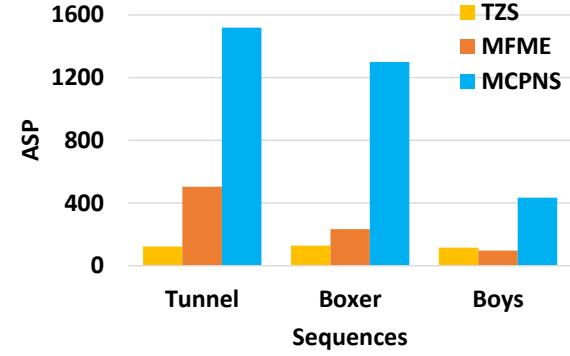
** It assumes that the videos sequences captured by plenoptic camera with the horizontal MLA orientation

method. More importantly, it should be noted that the coding performance of our method is better than the existing method and nearly comparable with the FS method, while our encoding time is much less.

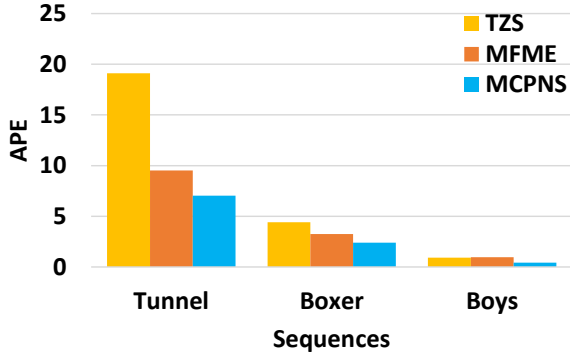
- In the case of without prior knowledge of MLA orientation, our method achieves significant performance gains compared to existing methods. For instance, the coding gain of our method over the MFME/MTSS is about 4.28%/1.25% and 2.63%/0.76% in the LD-Main and RA-Main conditions, respectively. Since the MFME/MTSS methods are set up to encode the plenoptic video sequences having the horizontal MLA configuration, which may fail to address the vertical MLA configuration in the Raytrix R5 and Single Focused camera models, as shown in Tables IV and V.
- In the case of knowing MLA information in advance, our method also achieves better performance gain compared to the MFME/MTSS. This is the case because our method has

additional search process around several key MCP locations to handle the large MV deviation in case of plenoptic 2.0 videos. Compared to MFME, the coding gain of our method is about 0.25%/0.35% in the LD-Main and RA-Main condition, respectively. In case of MTSS, although we cannot see the overall performance of the MTSS in case of with prior information of MLA orientation, we still observe that our method shows a better results on these video sequences capture by Raytrix R8 camera. In short, since the coding efficiency of MFME/MTSS is much lower compared to the FS method, these approaches might achieve sub-optimal performance compared to our method in the case of encoding plenoptic 2.0 videos.

- In terms of time complexity, our method does not achieve the fastest encoding time compared to existing methods, the encoding time of our method is competitive compared existing algorithms. For example, our method need about



(a) Average number of search points (ASP)



(b) Average of prediction errors (APE)

Fig. 13. A comparison of the average number of *ASP* and *APE* between various fast ME methods in several tested video sequences RA-Main, respectively.

3% and 5% of encoding time compared to TZS method. This is because our method spends more time on the neighbors MCP search process to handle the large motion deviation around MCP locations. Besides, thanks to our proposed fast search approach in MCP and its neighbors MCP locations, which enables our method to achieve the balance between the coding performance and encoding time complexity.

C. Ablation Study

1) *Average of Number of Search Points (ASP) and Average Prediction Error (APE)*: To measure the complexity of ME, we further calculate the average number of search points (*ASP*) for one ME, which is obtained as follows:

$$ASP = \frac{\sum_{i=1}^N SP(i)}{N} \quad (10)$$

where N denotes the times of ME and $SP(i)$ represents the number of search points in i -th ME. Moreover, we also evaluate the prediction accuracy of our proposed fast ME algorithm in terms of the average prediction error (*APE*), where the optimal MV is obtained by the FS method to measure the prediction error, as follows:

$$APE = \frac{\sum_{i=1}^N |MV_x^{Est}(i) - MV_x^{FS}(i)| + |MV_y^{Est}(i) - MV_y^{FS}(i)|}{N} \quad (11)$$

where N denotes the times of ME, and $MV^{Est}(i)$ and $MV^{FS}(i)$ denote the best MV estimated by the fast search method to be compared with the optimal MV obtained using the FS method

TABLE VI

THE ABLATION STUDY ON EFFECT OF DIFFERENT SEARCH LOCATIONS OF OUR METHOD IN RA-MAIN CONDITION

Methods	Combination of different search locations			
	(I)	(I)+(II)	(I)+(III)	(I)+(II)+(III)
Avg. BD-rate	-2.04%	-2.44%	-2.19%	-2.54%
Avg. Enc. Time	100	1.02	0.99	103%

(I) = MCP location; location (II) = Neighbors MCP location; (III) = Refinement location.

TABLE VII

THE ABLATION STUDY ON EFFECT OF DIFFERENT SEARCH CONFIGURATIONS OF OUR METHOD IN RA-MAIN CONDITION

Method	MLA orientation-agnostic search pattern		
	Original MCP Pattern	Hexagon Pattern	Rhombus Pattern
Avg. BD-rate	-2.67%	-2.28%	-2.54%
Avg. Enc. Time	106%	103%	103%

in i -th ME. The absolute difference error is calculated in the horizontal and vertical components of each MV. As shown in Fig. 13, we provide the *ASP* and *APE* measurements of the TZS, MFME, and our method in LD-Main and RA-Main, respectively. The results of the MTSS method are absent since we only have the executable file of this method. From these results, the number of search points in the proposed algorithms is higher than the TZS and MFME. However, it should be noted that our method has a smaller prediction error in terms of APE values compared to other methods, which means that our method can find better optimal MV resulting in better coding performance, as demonstrated in Tables IV and V.

2) *The effect of different configurations in our proposed method*. We present the results of the ablation study on the effect of key configurations in our proposed method in Tables VI, VII, and VIII. The following conclusions can be derived:

- *Without Neighbors MCP search*. To demonstrate the importance of our proposed neighbors MCP search. We present the turn-off test of different search locations in our proposed method as shown in Table VI. For the case of only searching MCP locations (i.e., search location (I)) or on MCP with refinement locations (i.e., search locations (I)+(III)), the performance dropped considerably compared to the original proposed method. For example, there are 0.50% and 0.35% of BD-rate losses compared to the originally proposed method. This was due to the fact that we failed to estimate the optimal MV, which has a large motion deviation around each MCP location. For the joint search locations MCP and its neighbors locations (i.e., search location (I)+(II)), the performance is nearly the same as our final method, which demonstrates the importance of our proposed neighbors MCP locations search to handle the larger MV deviation compared to existing MFME/MTSS methods.
- *Without Fast MCP Search*: To validate the contribution of fast MCP search, we present the performance between the

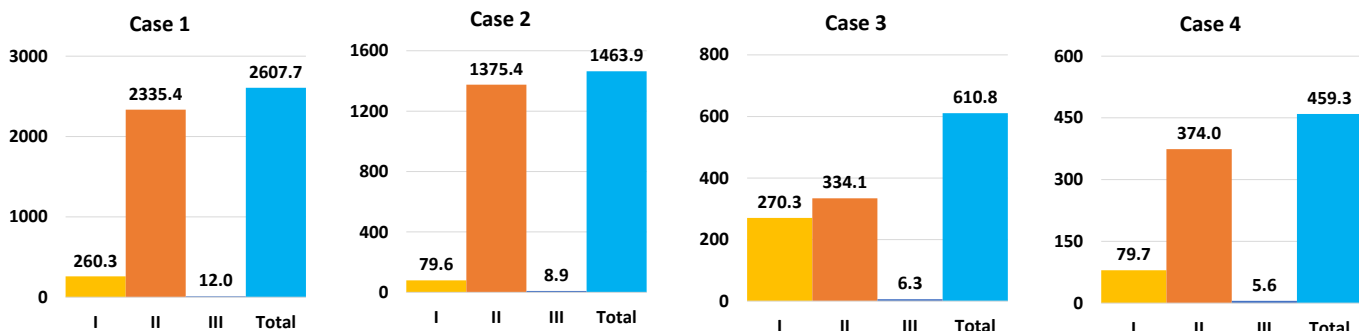


Fig. 14. Illustration the real time consumption and its portion in each searching step in the Tunnel sequence at QP35 at RA-Main condition. (I)- MCP search location, (II) Neighbors MCP search location; (III)-Refinement search location. (X-axis: search location, Y-axis: Time in second).

TABLE VIII

THE ABLATION STUDY ON EFFECT OF DIFFERENT FAST SEARCH CONFIGURATIONS OF OUR METHOD IN RA-MAIN CONDITION

Search level Case number	MCP search locations		Neighbors MCP search locations		Average BD-rate (%)	Average Encoding Time (%)
	Original search candidates	Fast search candidates	Original search candidates	Fast search candidates		
Case 1	O	X	O	X	-2.69%	115%
Case 2	X	O	O	X	-2.49%	107%
Case 3	O	X	X	O	-2.67%	106%
Case 4	X	O	X	O	-2.54%	103%

*The highlighted row is the final method that we adopted as a in our paper

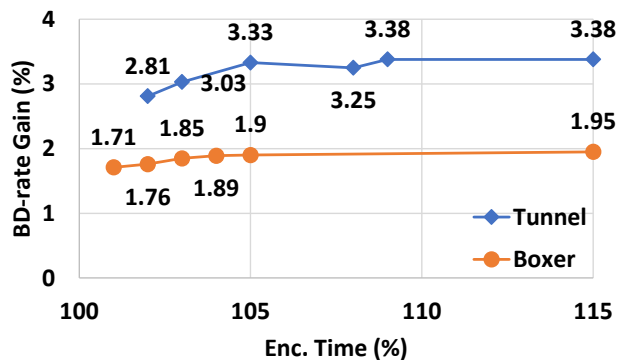


Fig. 15. An ablation tests on the parameter K number of neighbors MCP candidates, where there are five values of $K \in \{1, 2, 4, 8, 16, 32\}$ from the left to right of the diagram. In this paper, we adopted the $K = 16$ as the final setup.

original MCP search and fast MCP search patterns in Table VIII. It can be found the coding performance with our proposed fast MCP search enable (Cases 2 and 4) are little decreased compared to the testing cases using original MCP search pattern (Cases 1 and 3). However, when we enable our proposed fast MCP pattern as in the Cases 2 and 4, it can achieve considerable time savings compared to Cases 1 and 3 (e.g., the time complexity is reduced about three times, as shown in Fig. 14). It demonstrates that fast MCP search plays an important role in our proposed method. Moreover, we present the two possible fast MCP search pattern (e.g., hexagon vs rhombus), where the rhombus based fast MCP search shows better performance. Thus, we adopted the rhombus in our final method.

- *Without Fast Neighbors MCP Search:* A new test is present in the absence of our proposed fast neighbors MCP search. The results are also presented in Table VIII and Fig. 14. It can be found that the schemes without our fast neighbors MCP search consume significant additional computational power which needs to repeat the neighbors MCP search at every MCP location resulting in a huge encoding time increase. For example, about 3-5 times are increasing encoding time in neighbors MCP location searches when we compare the time consumption results between Case 1 with Case 3 (or Case 2 with Case 4). It should be noted that the coding performance is comparable compared to the original neighbors MCP search approach. Therefore, the proposed fast neighbors MCP search is indispensable to our proposed method. Besides, Fig. 15 illustrates the ablation tests on the effect of different K numbers of neighbors MCP search locations, where the performance is steadily increasing when the K is growing. However, for balance between performance and complexity, we finally adopted the $K = 16$ in this paper.

3) *Extend the Motion Estimation Process in Both-Predictive Search.* Bi-predictive motion estimation (BME) is carried out based on the results of uni-predictive motion estimation (UME), where the motion vector prediction (MVP) of the BME is set following the best estimated MV of each direction. The BME is used to obtain the optimal MV for each reference picture list: one is denoted as L0 (reference picture list 0) and the other as L1 (reference picture list 1). After that, the BME combines two blocks to predict the current block by using an averaged weight approach. In short, with a basic understanding of the motion estimation process, we can apply our proposed fast ME in both UME and BME. As shown in Table IX, our method achieves

TABLE IX

THE PERFORMANCE COMPARISON OF FAST ME METHODS USING IN BOTH-PREDICTIVE ME SEARCH WITH RA-MAIN CONDITIONS.

Camera model	Sequences	Applying in Uni-Predictive Search			Applying in Both-Predictive Search		
		MFME	MTSS*	MCPNS	MFME	MTSS*	MCPNS
Raytrix R5	Tunnel	0.37%	-3.38%	-3.38%	-1.00%	-3.11%	-4.03%
	Fujita	1.92%	-3.97%	-3.97%	-2.35%	-1.55%	-3.83%
	Origami	1.45%	-4.51%	-4.51%	-2.39%	-2.68%	-4.65%
	Leading	1.68%	-3.75%	-3.75%	-2.94%	-3.41%	-4.42%
Raytrix R8	Boxer	-1.63%	-1.90%	-1.90%	-1.67%	-1.84%	-2.80%
	ChessPieces	-4.41%	-4.64%	-4.64%	-4.55%	-4.44%	-5.21%
	ChessMoving	-3.38%	-4.75%	-4.75%	-4.63%	-5.46%	-5.87%
Single Focused	Boys	2.57%	-0.25%	-0.25%	1.88%	0.02%	-0.36%
	Experiments	1.40%	-0.64%	-0.64%	1.50%	-0.12%	-0.61%
	Cars	-0.03%	-0.03%	-0.03%	-0.08%	0.00%	-0.02%
	Matryoshka	1.04%	-0.08%	-0.08%	0.92%	-0.30%	-0.08%
Avg. BD-rate		0.09%	-1.78%	-2.54%	-1.39%	-2.08%	-2.90%
Avg. Enc. Time		99%	107%	103%	99%	109%	105%

*The results generated using an executable file provided by the authors, it only gives the best performance in case of sequences with the horizontal MLA orientation

more coding gains compared to the TZS anchor (i.e., VTM-11.0 anchor), where the BD-rate gains our method over the TZS are about 2.54%/2.90% when we apply our method in uni-predictive and both predictive search, respectively. Besides, our method yields coding gains of about 1.51%/0.82% compared to MFME[46]/MTSS[68] in RA-Main conditions, respectively. Based on the above test, it can be concluded that our proposed method brings considerable coding gain compared to other methods without requiring prior knowledge of MLA orientation.

V. CONCLUSIONS AND FUTURE WORKS

In this paper, we proposed a novel fast motion search algorithm for plenoptic 2.0 video coding. Based on the theoretical discussion and motion statistical analysis of 4D LF images, we first pointed out the main motion characteristic differences between the conventional and plenoptic videos, as well as the motion differences between MV generated by plenoptic 1.0 and 2.0 cameras. Then, we proposed an efficient search pattern to handle motion deviation for encoding plenoptic 2.0 videos. Our experiments verified the effectiveness of the proposed algorithm in terms of coding performance and computational complexity. Although our method achieves better coding performance compared to various state-of-the-art methods, the time complexity of the proposed method is still high. In the future, we will consider this aspect to design a simpler search pattern or an early skip ME method that can reduce the encoding time in specific application scenarios.

REFERENCES

- [1] G. Wu, et al., "Light field image processing: An overview," *IEEE J. Sel. Topics Signal Process.*, vol. 11, no. 7, pp. 926–954, Oct. 2017.
- [2] C. Conti, L. D. Soares, and P. Nunes, "HEVC-based 3D holoscopic video coding using self-similarity compensated prediction," *Signal Process., Image Commun.*, vol. 42, pp. 59–78, Mar. 2016.
- [3] Y. Li, M. Sjostrom, R. Olsson, and U. Jennehag, "Coding of focused plenoptic contents by displacement intra prediction," *IEEE Trans. Circuits Syst. Video Technol.*, vol. 26, no. 7, pp. 1308–1319, Jul. 2016.
- [4] R. J. S. Monteiro, P. J. L. Nunes, N. M. M. Rodrigues, and S. M. M. Faria, "Light field image coding using high-order intra block prediction," *IEEE J. Sel. Topics Signal Process.*, vol. 11, no. 7, pp. 1120–1131, Oct. 2017.
- [5] C. Conti, P. Nunes, and L. D. Soares, "Light field image coding with jointly estimated self-similarity bi-prediction," *Signal Process. Image Commun.*, vol. 60, pp. 144–159, Feb. 2018.
- [6] X. Jin, H. Han, and Q. Dai, "Image Reshaping for Efficient Compression of Plenoptic Content," *IEEE J. Sel. Top. Signal Process.*, vol. 11, no. 7, pp. 1173–1186, 2017.
- [7] X. Jin, H. Han, and Q. Dai, "Plenoptic image coding using macropixel-based intra prediction," *IEEE Trans. Image Process.*, vol. 27, no. 8, pp. 3954–3968, 2018.
- [8] L. Li, X. Jin, and T. Zhong, "Imaging-correlated intra prediction for plenoptic 2.0 video coding," in *2020 IEEE International Conference on Multimedia and Expo (ICME)*, 2020.
- [9] X. Jin, F. Jiang, L. Li, and T. Zhong, "Plenoptic 2.0 intra coding using imaging principle," *IEEE Trans. On Broadcast.*, vol. 68, no. 1, pp. 110–122, 2022.
- [10] E. Dib, M. Le Pendu, X. Jiang, and C. Guillemot, "Local low rank approximation with a parametric disparity model for light field compression," *IEEE Trans. Image Process.*, vol. 29, pp. 9641–9653, 2020.
- [11] M. Rizkallah, X. Su, T. Maugey, and C. Guillemot, "Geometry-aware graph transforms for light field compact representation," *IEEE Trans. Image Process.*, vol. 29, pp. 602–616, 2020.
- [12] G. De Oliveira Alves, et al., "The JPEG Pleno light field coding standard 4D-transform mode: How to design an efficient 4D-native codec," *IEEE Access*, vol. 8, pp. 170807–170829, 2020.
- [13] D. Liu, et al., "Pseudo-sequence-based light field image compression," in *Proc. IEEE Inter. Conf. on Multi. & Expo Workshops (ICMEW)*, 2016.
- [14] T. Nguyen Canh, V. V. Duong, and B. Jeon, "Boundary handling for view-based light field coding with a new hybrid scan order," in *Inter. Workshop on Adv. Image Tech. (IWAIT)*, 2019.
- [15] G. Wang, W. Xiang, M. Pickering, and C. W. Chen, "Light field multi-view video coding with two-directional parallel inter-view prediction," *IEEE Trans. Image Process.*, vol. 25, no. 11, pp. 5104–5117, Nov. 2016.
- [16] V. Avramelos, J. D. Praeter, G. V. Wallendael, and Lambert, P., "Random access prediction structures for light field video coding with MV-HEVC," *Multi. Tools and Applications*, vol. 79, pp. 12847–12867, May. 2020.
- [17] W. Tu, X. Jin, L. Li, C. Yan, Y. Sun, M. Xiao, W. Han, and J. Zhang, "Efficient Content Adaptive Plenoptic Video Coding," *IEEE Access*, vol. 8, pp. 5797–5804, Jan. 2020.
- [18] T. H. Nguyen, V. V. Duong, B. Jeon, "Random-access-aware Light Field Video Coding using Tree Pruning Method," in *Proc. IEEE Inter. Conf. Visual Commun. and Image Processing*, 2020, pp. 128–131.
- [19] N. Mehajabin, M. T. Pourazad, and P. Nasiopoulos, "An efficient pseudo-sequence-based light field video coding utilizing view similarities for prediction structure," *IEEE Trans. Circuits Syst. Video Technol.*, vol. 32, no. 4, pp. 2356–2370, 2022.
- [20] T. N. Huu, V. Van Duong, J. Yim, and B. Jeon, "Ray-space motion compensation for lenslet plenoptic video coding," *IEEE Trans. Image Process.*, vol. 32, pp. 1215–1230, 2023.

- [21] C. Conti, L. D. Soares, and P. Nunes, "Dense Light Field Coding: A Survey," *IEEE Access*, vol. 8, pp. 49244-49284, March. 2020.
- [22] C. Brites, J. Ascenso, and F. Pereira, "Lenslet Light Field Image Coding: Classifying, Reviewing and Evaluating," *IEEE Trans. Circuits Syst. Video Technol.*, vol. 31, no.1, pp. 339-354, Jan. 2021.
- [23] N00011, "Activity Report on Dense Light Fields", *132th MPEG meeting of ISO/IEC JTC1/SC29/WG11*, Online, October, 2020.
- [24] X. Jin, L. Li, T. Zhong, "Exploration of Lenslet Data Compression", *ISO/IEC JTC1/SC29/WG11 MPEG2018/M44685*, Macao, China.
- [25] Fan Jiang, Xin Jin, Tingting Zhong, "Exploration Experiment of Plenoptic 2.0 test sequences for Dense Light Field Compression and Summary of Performance", *ISO/IEC JTC1/SC29/WG11 MPEG2020/M52249*, Brussels, Belgium January 2020.
- [26] Xin Jin, Kedeng Tong, Euee S. Jang, Toshiaki Fujii, Gauthier Lafruit, Mehrdad Teratani, "Draft Use Cases and Requirements of Lenslet Video Coding (LVC) for Dense Light Fields (DLF)", *ISO/IEC JTC 1/SC 29/WG 2 N167*, January 2022.
- [27] S. Fujita, S. Mikawa, M. Teratani, K.Takahashi, and T.Fujii "Extracting Multi-View Images from Multi-Focused Plenoptic Camera". in *Proc. Inter. Workshop on Advanced Image Technology (IWAIT) 2019*.
- [28] M. Teratani, S. Fujita, W. Ouyang, K. Takahashi, and T. Fujii "3D Imaging System Using Multi-Focus Plenoptic Camera and Tensor Display", *International Conference on 3D Immersion (IC3D2018)*.
- [29] S. Fachada, D. Bonatto, A. Losfeld, G. Lafruit, and M. Teratani, "Pattern-free Plenoptic 2.0 Camera Calibration", in *Proc. IEEE 24th International Workshop on Multimedia Signal Processing MMSP*.
- [30] S. Fachada, A. Losfeld, T. Senoh, G. Lafruit, and M. Teratani, "A Calibration Method for Subaperture Views of Plenoptic 2.0 Camera Arrays", in *Proc. Inter. Workshop on Multi. Signal Process. MMSP 2021*.
- [31] J. Jain and A. Jain, "Displacement measurement and its application in interframe image coding," *IRE Trans. Commun. Syst.*, vol. 29, no. 12, pp. 1799-1808, 1981.
- [32] T. Koga, A. Hirano, J. Ohki, and K. Iinuma, "Motion-compensated interframe coding for video conference," *ITE Technical Report*, vol. 5, no. 9, pp. 85-90, 1981.
- [33] R. Li, B. Zeng, and M. L. Liou, "A new three-step search algorithm for block motion estimation," *IEEE Trans. Circuits Syst. Video Technol.*, vol. 4, no. 4, pp. 438-442, 1994.
- [34] L.-M. Po and W.-C. Ma, "A novel four-step search algorithm for fast block motion estimation," *IEEE Trans. Circuits Syst. Video Technol.*, vol. 6, no. 3, pp. 313-317, 1996.
- [35] L.-K. Liu and E. Feig, "A block-based gradient descent search algorithm for block motion estimation in video coding," *IEEE Trans. Circuits Syst. Video Technol.*, vol. 6, no. 4, pp. 419-422, 1996.
- [36] S. Zhu and K. K. Ma, "A new diamond search algorithm for fast block-matching motion estimation," *IEEE Trans. Image Process.*, vol. 9, no. 2, pp. 287-290, 2000.
- [37] C. Zhu, et al., "A novel hexagon-based search algorithm for fast block motion estimation," in *Proc. IEEE Inter. Conf. on Acoustics, Speech, and Signal*, 2002.
- [38] M.Tourapis, O.C.Au, M.L.Liou, "Fast Block Matching Motion Estimation using Predictive Motion Vector Field Adaptive Search Technique". *ISO/IEC/JCT1/SC29/WG11 MPEG2000/M5866*, 2000
- [39] Zhibo Chen, Peng Zhou, Yun He. "Fast Integer Pel and Fractional Pel Motion Estimation for JVT", *Joint Video Team (JVT) of ISO/IEC MPEG & ITU-T VCEG*, December, 2002.
- [40] G. J. Sullivan, et al., "Overview of the high efficiency video coding (HEVC) standard," *IEEE Trans. Circuits Syst. Video Technol.*, vol. 22, no. 12, pp. 1649-1668, 2012.
- [41] S. Ma, B. M. Smith, and M. Gupta, "3D scene flow from 4D light field gradients," in *Proc. ECCV 2018*, pp. 681-698.
- [42] A. Lumsdaine and T. Georgiev, "The focused plenoptic camera," in *Proc. IEEE Inter. Conf. on Computational Photography (ICCP)*, 2009, pp. 1-8.
- [43] M. Levoy and P. Hanrahan, "Light field rendering," in *23rd Annual Conf.on Computer Graphics and Interactive Techniques*, in *Proc. SIGGRAPH*, 1996, pp. 31-42.
- [44] S. Gortler, R. Grzeszczuk, R. Szeliski, and M. Cohen, "The lumigraph," in *Proc. SIGGRAPH*, 1996, pp. 43-54.
- [45] F. Bossen, Common Test Conditions and Software Reference Configurations, *JCT-VC, doc. JCTVC-I1100*, May 2012.
- [46] L. Li, X. Jin, H. Han, and Q. Dai, "Macropixel based Fast Motion Estimation for Plenoptic Video Compression" *Pacific-rim Conf. Multimedia*, vol. 3, pp. 730-739, 2018.
- [47] L. Li, and X. Jin, "Macropixel-constrained Collocated Position Search for Plenoptic Video Coding," *Proc. IEEE Inter. Conf. Visual Comm. and Image Processing*, 2020, pp. 1-4.
- [48] Xin Jin, Lingjun Li, Tingting Zhong, "Exploration of Lenslet Data Compression", *ISO/IEC JTC1/SC29/WG11 MPEG2018/M44685*, Macao, China.
- [49] X. Jin, C. Wang, K. Tong, "Summary of evidence in lenslet coding", *ISO/IEC JTC1/SC29/WG11 MPEG2021/M56790*, Online.
- [50] Y. Yu, X. Jin, C. Wang, K. Tong, C. Wang, "[LVC][DLF] Integrated coding tools for the lenslet video on HEVC", *ISO/IEC JTC1/SC29/WG11 MPEG2022/M60183*, Online.
- [51] T. N. Huu, V. Van Duong, and B. Jeon, "Fast and efficient microlens-based motion search for plenoptic video coding," in *2021 IEEE International Conference on Image Processing (ICIP)*, 2021.
- [52] Y. Yim, T. N. Huu, and B. Jeon, "[LVC][DLF] Fast and efficient microlens-based motion search for Lenslet Video Coding", *ISO/IEC JTC1/SC29/WG11 MPEG2022/M60992*, Online.
- [53] Y. Yu, X. Jin, C. Wang, K. Tong, "[LVC][DLF] Improved Test Zone Search for Plenoptic 2.0 video coding", *ISO/IEC JTC1/SC29/WG11 MPEG2022/M60995*, Online.
- [54] Yuqing Yang, Xin Jin, Chen Wang, Kedeng Tong, Haitian Huang, "Micro-image Correlative Block Search for Plenoptic 2.0 video coding", *ISO/IEC JTC1/SC29/WG4 MPEG2022/M60997*, Online.
- [55] Yuqing Yang, Xin Jin, Chen Wang, Kedeng Tong, Haitian Huang, "Microimage-based Two-step Search for Plenoptic 2.0 Video Codings", *ISO/IEC JTC1/SC29/WG4 MPEG2022/M61861*, Online.
- [56] Chen Wang, Xin Jin, Kedeng Tong, Yuqing Yang, "Integrated coding tools for the lenslet video on VVC", *ISO/IEC JTC1/SC29/WG4 MPEG2022/m60996*, Online.
- [57] K. Tong, X. Jin, F. Jiang, T. Zhong, C. Wang, "[DLF] Transfer the inter coding tool for lenslet video compression to VVC", *ISO/IEC JTC1/SC29/WG4 MPEG2021/M56785*, Online.
- [58] VVC reference software VTM-11.0 [Online]. Available at https://vcgit.hhi.fraunhofer.de/jvet/VVCSoftware_VTM/-/tags/VTM-11.0
- [59] Exploration Experiments and Common Test Conditions for Dense Light Fields, *ISO/IEC JTC 1/SC 29/WG 04, MDS20009_WG04_N00057*, Online, January 2021.
- [60] Overview of MPEG-I Visual Test Materials, *ISO/IEC JTC 1/SC 29/WG 04, MDS20005_WG04_N00053*, Online, January 2021.
- [61] G. Bjontegaard, "Calculation of average PSNR differences between RDcurves," *ITU-T SG16 Q.6, VCEG-M33, VCEG of ITU-T, Austin, Texas, USA, Tech. Rep. VCEG-M33*, Apr. 200.
- [62] Jonghoon Yim, Vinh Van Duong, Thuc Nguyen Huu, Byeungwoo Jeon, "[LVC][DLF] Fast and Efficient Macropixel Collocated Pixel Search for Plenoptic 2.0 Video Coding", *ISO/IEC JTC 1/SC 29/WG 4 MPEG2023/M63315*, Antalya, Turkey, April 2023.
- [63] Yuqing Yang, Xin Jin, Kedeng Tong, Chen Wang, Haitian Huang, "[DLF] [LVC] Updated Performance of Microimage-based Two-step Search for Plenoptic 2.0 Video Coding," *ISO/IEC JTC 1/SC 29/WG 4 m62934*, Antalya, Turkey, April 2023.
- [64] Jingyang Luo, Jiedong Ye, Qiong Liu, You Yang, "[LVC][DLF] Macropixel level and pixel level mixed search for plenoptic 2.0 videos", *ISO/IEC JTC 1/SC 29/WG 4 MPEG2023/M63160*, Antalya, Turkey, April 2023.
- [65] Jingyang Luo, Jiedong Ye, Qiong Liu, You Yang, "[LVC][DLF] Macropixel-constrained Collocated Position Layered Search for Plenoptic 2.0 Videos", *ISO/IEC JTC 1/SC 29/WG 4 MPEG2023/M64075*, Geneva, Switzerland, July 2023.
- [66] Yuqing Yang, Xin Jin, Kedeng Tong, Chen Wang, "[LVC] [DLF] Low-complexity Microimage-based Two-step Search for Plenoptic 2.0 Video Coding", *ISO/IEC JTC 1/SC 29/WG 4 MPEG2023/M64053*, Geneva, Switzerland, July 2023.
- [67] Jonghoon Yim, Vinh Van Duong, Thuc Nguyen Huu, Byeungwoo Jeon, "[LVC][DLF] Improving Macropixel Collocated Position Search for Plenoptic 2.0 Video Coding", *ISO/IEC JTC 1/SC 29/WG 4 MPEG2023/M63908*, Geneva, Switzerland, July 2023.
- [68] Y. Yang, X. Jin, K. Tong, C. Wang and H. Huang, "Microimage-based Two-step Search For Plenoptic 2.0 Video Coding," in *Proc. IEEE International Conference on Multimedia and Expo (ICME)*, 2023, pp. 2567-2572.